Chemical Engineering Journal 545 (2026) 179153

Contents lists available at ScienceDirect

Chemical Engineering Journal

journal homepage: www.elsevier.com/locate/cej

A safety-driven approach for the scale-up of membrane production processes

Benedetta A. De Liso [a], Clara Coiana [b], Gianmaria Pio [a], Fausto Gallucci [b,c], Ernesto Salzano [a,*]

[a] LISES – Laboratory of Industrial Safety and Environmental Sustainability, Department of Civil, Chemical, Environmental and Materials Engineering (DICAM), University of Bologna, Italy
[b] SPE – Sustainable Process Engineering, Department of Chemical Engineering and Chemistry, Eindhoven University of Technology, the Netherlands
[c] ZEFIRA BV – Kastanjelaan 400, 5616 LZ, Eindhoven, Netherlands

ARTICLE INFO

Keywords:
Process scale-up
Fire safety
Membranes
Matrix of interactions
Cone calorimeter

ABSTRACT

The development and scale-up of innovative chemical processes require the simultaneous optimisation of performance, sustainability, and safety. However, safety is often marginally considered in early-stage design, leading to suboptimal scale-up. In this work, a phenomenology-driven methodology is proposed for inherent safety assessment by integrating mechanistic interaction mapping with targeted experimental validation. The approach combines identification of key monitoring and influencing parameters with production of interaction matrices and controlled thermal-stress data to detect critical process–material interactions at low technology readiness levels. The methodology was applied to novolac-based carbon membranes, focusing on replacing *N*-methyl-2-pyrrolidone (NMP) with γ-valerolactone (GVL). Cone calorimeter tests (7–50 kW/m^2) were conducted to assess ignitability, flame behaviour, and exhaust emissions. The novolac/NMP system showed rapid ignition and sustained combustion, with peak heat release rates above 1000 kW/m^2. In contrast, novolac/GVL exhibited reduced ignition propensity (~10–15%) and lower smoke and CO emissions (up to ~30%), as quantified through normalised safety-ranking indicators derived from cone calorimeter measurements (based on time-to-ignition, heat release rate, mass loss rate, and gas emission metrics), while maintaining similar thermal activation of the polymer. These results demonstrate that the proposed framework enables comparison of alternative formulations by jointly addressing performance and safety under thermal stress, supporting safer and more sustainable early-stage process design.

1. Introduction

The current need for sustainable processes and products has promoted the development and scale-up of alternative industrial routes and materials. The successful implementation of an innovative solution is a multi-step process requiring an interdisciplinary perspective. Scaling up an industrial process from laboratory scale involves the careful transition from small-scale experimental setups to full production systems, while ensuring consistency, safety, and economic viability [1]. This process demands rigorous evaluation of equipment design, material handling, and reaction kinetics, which often behave differently once reactor size or layout is changed [2]. Engineers must account for changes in heat and mass transfer, process control, and potential risks that may not be evident in the laboratory [3]. To properly address this challenge, the use of validated models and correlations is essential. Additionally, regulatory compliance, cost optimisation, and market demand play critical roles in shaping decisions during scale-up, requiring close collaboration across technical and business experts [3]. Nevertheless, in most cases, the research activities in an early stage focus on the identification and optimisation of operative conditions and models required for the equipment design and cost estimation, with a limited role for the safety aspects. Once included in the analysis, the safety in early-stage design phases is typically devoted to the comparison of production processes and supply chains of alternative products, based on the amount of hazardous materials employed by the expected list of equipment items [4]. This approach, however, overlooks the hazards that may arise from reactivity, as well as the formation of intermediates and products from unwanted reactions. In this light, the inclusion of reactivity-related hazards in early-stage analyses is recommended to guide and support the selection of inherently safer

* Corresponding author.
E-mail address: ernesto.salzano@unibo.it (E. Salzano).

https://doi.org/10.1016/j.cej.2026.179153
Received 14 April 2026; Received in revised form 19 June 2026; Accepted 5 July 2026
Available online 6 July 2026

technological solutions. In this regard, several strategies can be implemented within the concept of "safe by design", including process intensification or minimising storage of hazardous materials, substitution with less hazardous substances, attenuation or moderation through the use of less hazardous conditions, and mitigation of consequences employing protective systems and barriers [5]. To assess the reactivity hazards of chemicals, a large variety of indicators based on the properties of the substances have been proposed (e.g., Oxygen balance, reaction hazard index, thermal risk index, and NFPA rating). However, these approaches intrinsically suffer from a lack of information related to the operative conditions, interactions between components of mixtures, and layout of the equipment items considered [6], which can be particularly relevant within the chemical and process industries. A clear example of this case is associated with processes dealing with exothermic reactions (e.g., partial oxidations), potentially prone to runaway reactions, which can result in overpressure as well as the formation of unstable, flammable and/or toxic species within the reactors. Several approaches and criteria have been developed and defined for the quantification of the risk of runaway reactions, accounting either for operative conditions potentially leading to hazardous scenarios or consequences of the occurrence of undesired reactions. As a way of example, stability-based criteria (e.g., Semenov-criterion, Lyapunov-stability, and Strozzi-Zaldivar criterion), geometry-based criteria (e.g., Adler and Enig criterion, Maxi criterion, adiabatic criterion), and sensitivity-based criterion (i.e., Morbidelli-Varma criterion) are worth mentioning, as described in the dedicated literature [7]. Although these approaches can be implemented for a proper design and optimisation of an industrial facility as well as early warnings of existing plants [8], the use of the Westerterp number is considered a key parameter when dealing with the scale-up from laboratory reactors to industrial scale technologies since it includes the overall heat transfer coefficient, heat transfer area, volume, density, and heat capacity at the initial conditions as well as the dosing time and the relative increase in volume [7,9]. Considering the parameters involved, a preliminary design of the system is needed, including the cooling/heating systems. Therefore, the quantification of the Westerterp number can conveniently guide the transition from technological readiness levels TRL 4 (i.e., validation in a laboratory environment) to TRL 6 (i.e., validation in an industrial environment) or larger. However, the use of the Westerterp number and similar scale-up criteria requires detailed information on process configuration, operating conditions, and heat-transfer systems, which is often unavailable at low TRLs. The methodology proposed in this work complements these approaches by supporting the identification of inherently critical process-material interactions and safety-relevant phenomena before detailed process design becomes available.

To support the scientific research through the previous steps of the scale-up process, alternative approaches based on the theoretical and empirical knowledge of the possible interactions between components at relevant operative conditions are recommended. Among the others, the use of the interaction matrix [10] is worth considering. In this case, the possible intended and unintended reactions between materials and energy sources involved in a chemical process are analysed. Considering the type of information required, this approach applies to any stage of the process life cycle, including laboratory-scale and full-scale industrial plants. In this sense, the creation of a checklist, guiding the analysis, is recommended to guarantee systematic and robust investigations. In the context of an interaction matrix, the inclusion of a broad number of chemicals and energy sources significantly increases the dimensionality of the resulting matrices, posing challenges to both efficiency and interpretability of the results. As a result, there is a tendency to preselect components based on their classification as hazardous materials, thus narrowing the scope of evaluation. Indeed, such an approach may lack conservatism, particularly when dealing with polymers. Unlike their parent compounds, polymer degradation products may exhibit significant hazard either in terms of flammability or toxicity, suggesting dedicated studies on the subject [11,12]. To this aim, fire testing techniques can provide essential elements for the inclusion of materials within the safety analyses. A widely used method is the Limiting Oxygen Index (LOI), which determines the minimum concentration of oxygen needed to sustain a flame. Materials with higher LOI values are generally more resistant to ignition [13]. Similarly, UL-94 tests aim to classify the materials based on their response to exposure to a test flame under controlled conditions [14]. Cone calorimetry is particularly valuable, measuring key parameters such as heat release rate, mass loss rate, time to ignition, and smoke production [15]. Complementing this, thermogravimetric analysis (TGA) reveals decomposition patterns by heating samples in controlled atmospheres. This technique, especially when combined with FTIR or mass spectrometry, helps identify the volatile compounds produced during thermal decomposition. For these reasons, the present work reports an innovative and comprehensive methodology based on the evaluation of chemical interactions to guide the development and scale-up of industrial processes. The capabilities and limitations of the proposed protocol are illustrated through its application to a case study examining the production process of novolac-based carbon membranes. Over the past few decades, this class of membranes has emerged as a particularly promising technology for hydrogen separation and purification, CO_2 separation, and water separation in membrane reactors offering a more sustainable alternative to conventional methods such as cryogenic distillation [16–19].

Employing a safety-driven approach to support the scale-up of carbon membrane manufacturing can therefore provide a valuable contribution to the energy transition, enabling the broader adoption of cleaner energy carriers such as hydrogen.

2. Methodology

To systematically identify and assess the most relevant aspects to include in the development of innovative technological solutions and processes, a stepwise workflow consisting of five steps identified under the acronym SCALE was proposed, as reported in Fig. 1. The approach is grounded in a rigorous identification and classification of system parameters, enabling a structured evaluation of both performance and safety-relevant outcomes. The developed protocol was tested in a case study aiming at optimising the production of novolac-based carbon membranes (CMs). For the sake of clarity, specific information on the defined steps is provided in the subsequent sections, together with the practical elements associated with the selected case study, once relevant.

Step 1 – Selection of variables: An innovative solution can be identified as a potential target for further research and development stages, based on the optimisation of a given set of target parameters. Once the target processes/products are selected, the potentially relevant characteristics and variables shall be identified, avoiding redundant or overlapping descriptors to ensure clarity, independence, and comprehensive coverage of system behaviour.

Application: As concerns the case study under development, the transition toward more sustainable and efficient chemical processing technologies has been intensified in recent years, driven by increasingly stringent environmental regulations and a growing demand for decarbonised energy systems. In this context, membrane-assisted reactors (MRs) have emerged as a pivotal innovation, offering an integrated platform in which chemical reactions and selective separations can occur simultaneously within a single unit or in separated units. This coupling not only enhances conversion efficiency by continuously removing products or inhibiting species but also minimises downstream purification needs, ultimately contributing to lower energy consumption and reduced process intensification costs [20]. The quality of CMs is assessed through the selectivity and permeance to a given species, which have been considered as target parameters in this study. The production of CMs involves a multi-step process that starts with the selection/synthesis of polymeric precursors, which are processed into a specific morphology (e.g., hollow fibres or flat sheets) before undergoing

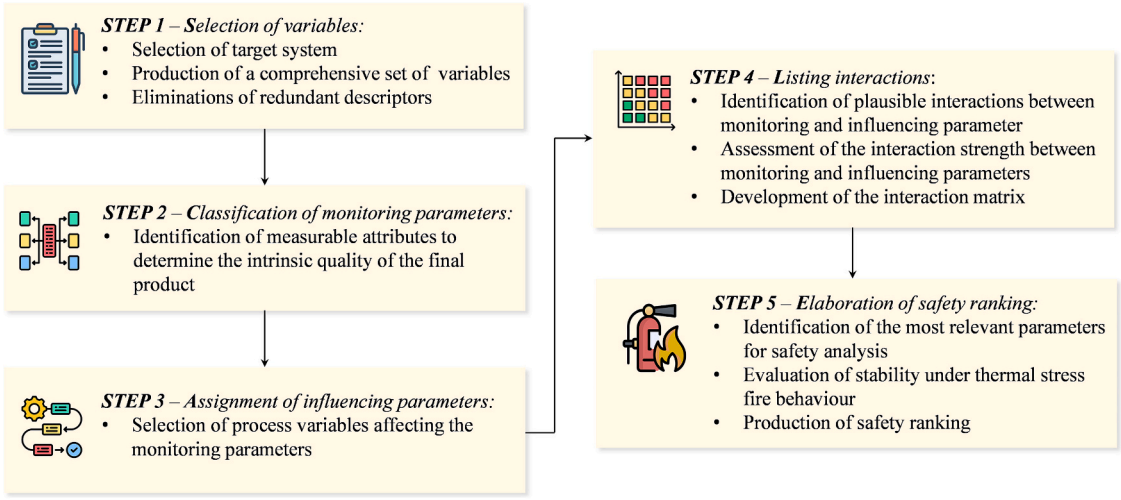

Fig. 1. Workflow for the systematic assessment of process–material interactions based on the proposed SCALE approach, including monitoring and influencing parameter definition, mechanistic interaction mapping and safety evaluation.

thermal treatment [21,22]. Among the various precursors available, Novolac resins, which belong to the family of phenolic polymers, are widely used due to their aromatic structure which leads to high thermal stability and carbon yield. This case study refers to the Novolac based membranes, but can be extended to all CMs.

Step 2 – Classification of monitoring parameters: Monitoring parameters can be defined as measurable attributes directly reflecting intrinsic quality, encompassing structural organisation, dimensional features, surface morphology, chemical composition, and mechanical integrity. Each monitoring parameter can be selected based on reproducibility, sensitivity to process variations, and capacity to capture meaningful changes in the system state.

Application: In this step, the focus is on selecting measurable monitoring parameters that reflect the final membrane quality. Given the strong dependence of the final membrane performance on the structural and chemical transformations occurring during thermal treatment, a rigorous evaluation of the quality of the product requires identifying which physical characteristics are most indicative of its final functionality. In this context, a set of measurable monitoring parameters capturing pore structure, morphological uniformity, surface features, and chemical composition can be used to quantitatively describe the final state.

Step 3 – Assignment of influencing parameters: A preliminary description of a possible production process is needed at this stage to identify influencing parameters among operational conditions, process variables, and layout employing a mechanistically justified causal effect on the monitoring parameters. In other words, a significant variation in at least one monitoring parameter can be attributable to a property of the investigated systems to be defined as an influencing parameter.

Application: In Step 3, key process and material variables affecting the monitoring parameters from Step 2 are identified. For CMs, these parameters are closely linked to the thermal treatment of Novolac-based precursors. These thermosetting materials exhibit excellent thermal stability, making them ideal for pyrolysis, a critical step in membrane production [23]. The process begins with the polymer precursor being dissolved in an appropriate solvent, forming a solution whose rheology can be tuned to facilitate casting or spinning. This solution is then shaped into the desired form, such as tubular, hollow fibres, or flat sheets, often supported on an appropriate substrate, before undergoing carbonisation at elevated temperatures (450 °C - 1000 °C) under an inert atmosphere. This thermal treatment leads to the formation of a microporous (< 2 nm) and ultra-microporous (< 0.6 nm) carbon network, characterised by a narrow pore size distribution that is essential for precise hydrogen separation [24,25]. The pyrolysis conditions, including temperature, heating rate, and atmosphere conditions, must be tightly controlled to optimise the performance of membranes. Any deviation in these parameters can significantly impact the final product, compromising its separation properties and structural integrity [26,27]. In this framework, the polymer type is treated as a fixed independent variable, providing a constant chemical baseline. The influencing parameters, therefore, correspond exclusively to the controllable elements of the fabrication and thermal-treatment process. Among these, the solvent system, defined by its polarity, coordination ability, and volatility, acts as the primary lever shaping precursor organisation [28]. Solution rheology, casting conditions, additive selection, and the full thermal-treatment schedule (heating rate, dwell time and final temperature) further modulate the structural evolution of the material [29,30]. Additionally, support selection plays a critical role in ensuring mechanical stability and limiting defect formation during processing. Together, these variables delineate the process space governing the monitoring parameters introduced in Step 2.

Step 4 – Listing interactions: For each monitoring–influencing pair, the dominant physical or chemical process was determined, considering transport limitations, structural evolution, stress development, thermal responses, and decomposition pathways. Interaction strengths (Strong / Medium / Weak) were assigned based on relative magnitude and dominance of the observed trends, theoretical plausibility, literature and experimental evidence. Given the absence of a universally accepted quantitative framework for interaction ranking in carbon membrane processing, and the inherent variability of fabrication routes and operating conditions reported in the literature, the REC approach is intentionally formulated as a semi-quantitative methodology. This choice enables a consistent comparison of interactions across different process configurations while maintaining sufficient flexibility to account for system-specific mechanistic and experimental evidence. Mechanistic relevance (R) considers how directly parameter A influences parameter B, with scores ranging from 0 for indirect or mechanical effects, 1 for plausible effects, and 2 for direct and clearly established influence. For each interaction, mechanistic relevance is first assessed based on the existence of a physically or chemically justified coupling between parameters. Magnitude or expected effect (M) reflects the expected impact of parameter A on the functional outcome of interest, scored as 0 for negligible, 1 for moderate, and 2 for significant effects. It is determined by evaluating the sensitivity of the monitored variable to variations in the influencing parameter, using experimental trends or literature-reported ranges when available. Consistency or confidence (C) is assigned based on the agreement between mechanistic expectations, literature evidence, and experimental observations from the present

Table 1
Definitions and scoring scheme for the assessment of interaction strengths in the evaluation matrices.

Criterion	Definition	Scoring
R – Mechanistic relevance	The degree to which parameter A directly influences parameter B	0 = indirect/mechanical effect 1 = plausible effect 2 = direct and clear influence
E –Expected effect / Magnitude	Expected impact of parameter A on functional outcome	0 = negligible 1 = moderate 2 = significant
C – Consistency / Confidence	Reliability and reproducibility of the effect	0 = theoretical only / no data 1 = supported by proxy or literature 2 = proved by multiple sources or clear experimental data

study. More specifically, it captures the reliability of the observed or anticipated interaction, based on experimental data, literature evidence, or mechanistic proxies, scored as 0 if only theoretical, 1 if supported by literature or proxies, and 2 if confirmed by multiple sources or clear experimental observations. The sum of these three scores (ranging from 0 to 6) was then mapped to qualitative interaction strengths: Strong for scores of 5–6, Medium for 3–4, and Weak for 0–2. This sequential procedure ensures that each criterion is evaluated independently and reduces ambiguity in the scoring process. Additional information about the sub-criteria and the rating score procedure adopted can be found in the supplementary material. Controlled heat-flux testing (as detailed in the following section) offered additional experimental context, particularly for those interactions associated with potential thermal instability, rapid mass loss, or exothermic events. In this way, the framework effectively integrates mechanistic reasoning, expected functional impact, and reproducibility, establishing a robust method for quantifying parameter interactions in a generalizable and reproducible manner. A summary of this evaluation framework, including definitions and scoring criteria for Mechanistic relevance (R), Expected effect (E), and Consistency (C), is presented in Table 1.

Following the established workflow, the Monitoring ↔ Monitoring and Influencing ↔ Monitoring matrices can be constructed and populated with interaction strengths derived from theoretical considerations, material descriptors, and internal consistency checks. Redundancies must be eliminated at this stage, and each interaction shall be retained only when supported by a clearly identifiable physical or chemical mechanism. The concurrent analysis of monitoring and influencing parameters naturally enabled the identification of the critical stage of the process, defined as the condition in which the material becomes most sensitive to thermal exposure and compositional changes. This stage was recognised by the convergence of multiple strong interactions, particularly those associated with mass-loss propensity, thermal decomposition behaviour, and the evolution of volatile species, thus providing the logical focal point for subsequent safety-related considerations. Building on this outcome, a dedicated safety evaluation was incorporated as the final element of the methodology.

Step 5 – Elaboration of safety ranking: Safety-relevant interactions were isolated by screening for parameter combinations indicative of potential hazards under external heat flux, such as accelerated devolatilisation, early-stage decomposition, and rapid changes in heat-release behaviour. A targeted experimental campaign was executed to substantiate the safety-relevant interaction nodes emerging from the interaction matrices and to provide quantitative evidence of material response under controlled thermal loading. The experimental strategy employed a bench-scale cone calorimeter (Fig. 2) as a reproducible, well-characterised radiant-heating environment capable of producing the external heat fluxes representative of the critical stage previously identified by the workflow. Tests were therefore designed to probe the thermal and devolatilisation behaviour of the material and to map the transient phenomena that inform interaction strength assignments (e.g., early volatilisation, multi-step mass-loss, surface heterogeneity, and anomalous heat-release events).

In this work, the experimental tests were carried out at imposed radiant heat fluxes in the range 7, 25, and 50 kW/m^2, under controlled ventilation and sample mounting conditions consistent with the

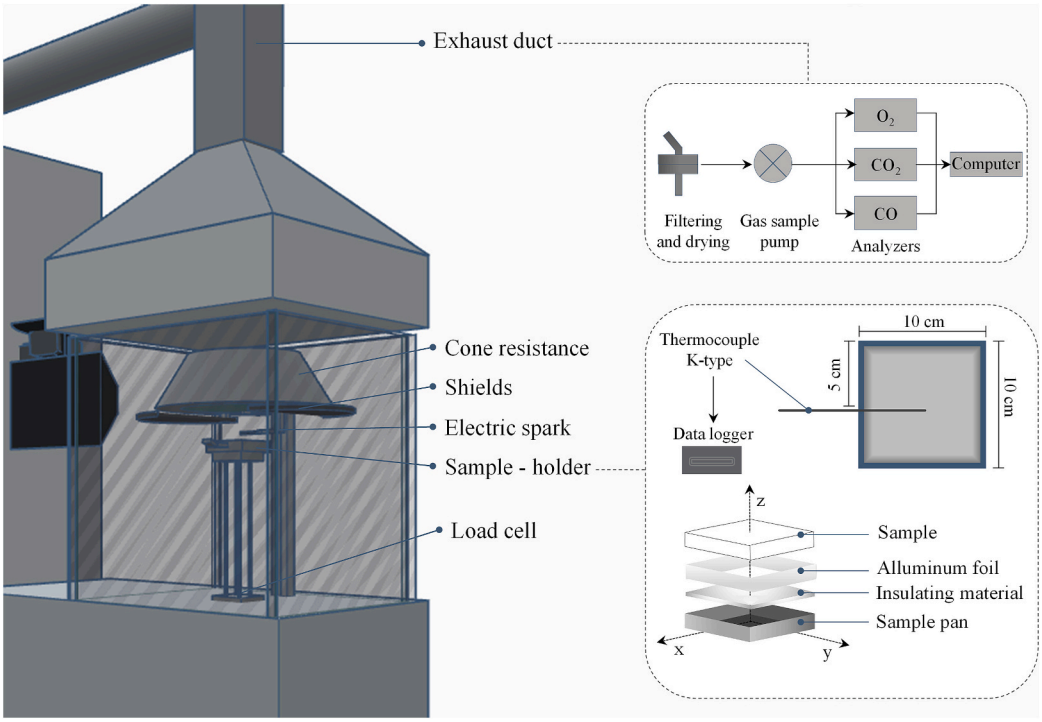

Fig. 2. Schematic representation of the experimental system adopted in this work.

standard procedure [31]. Each specimen was placed in a stainless-steel sample holder; a K-type thermocouple was embedded into the holder immediately beneath the sample plane to record in-depth temperature profiles with high temporal resolution. All the experimental cone calorimeter tests were conducted three times for each set of conditions, the reported profiles are the average values of the measurements collected under the same conditions. In addition, the reliability and reproducibility of the results obtained by the implemented experimental protocol have been extensively validated and evaluated in previous investigations, available in the current literature [32]. Surface thermal behaviour was monitored by a Hikmicro infrared camera (spectral range 7–14 μm; NETD <35 mK; 25 Hz frame rate). The thermal camera was mounted laterally, outside the principal radiant cone, at a distance and angle selected to (i) avoid direct exposure to the heater and optical saturation, (ii) obtain an unobstructed full-field view of the exposed surface, and (iii) minimise reflections from metallic surfaces. Camera emissivity settings were calibrated against the embedded thermocouple before each test to enable quantitative surface-temperature mapping. Where applicable, gravimetric mass-loss traces and calorimetric outputs (heat release rate, HRR) were recorded continuously by the cone calorimeter's data acquisition system. Smoke production was quantified by the built-in laser photometric system, and gas outputs were sampled for downstream analysis when required. The combined instrument suite delivered the following time-resolved diagnostics: (i) heat release rate (HRR) as a proxy for energetic response, (ii) mass-loss rate (MLR) and cumulative mass loss for volatilisation and residue formation, (iii) time-to-ignition (TTI) or onset of sustained thermal decomposition, (iv) in-depth temperature profiles from the embedded thermocouple (T_C), and (v) spatial surface temperature fields (T_{surf}) and hotspot dynamics from infrared thermography. In addition, (vi) the flow rates of CO and CO_2 (COP and CO_2P) in the exhaust gases were continuously measured, providing a quantitative assessment of the fraction of the main volatilized material converted into gaseous products. Further information on the cone calorimeter apparatus and the adopted experimental procedure can be found elsewhere [33–35].

Based on the collected diagnostics, three principal aspects were considered for the safety ranking: *Ignitability*, *Flame behaviour*, and *Exhaust gases*. For each aspect, indicators were evaluated from both a mass-based perspective, which reflects the energetic and material consumption behaviour, and a thermal-based perspective, which captures the temperature evolution and heating dynamics within the sample and surrounding environment.

- For the *Ignitability*, the onset of sustained decomposition was characterised by the time-to-ignition measured in the cone calorimeter, as well as the temperature difference at the liquid–vapor interface recorded by the infrared camera and the liquid temperature by the thermocouple measurement ($\Delta T = T_{surf} - T_C$), providing complementary mass and thermal-based insights. Additionally, the temperature values were considered at the moment of ignition. Extended infrared thermography outputs, including representative thermal images, are provided in the supplementary material.
- The *Flame behaviour* was evaluated using both mass and thermal-based indicators. From the mass perspective, the peak mass-loss rate (pMLR) and the average value of the effective heat of combustion (EHC) were considered, capturing the rapidity and energy of material consumption. From the thermal perspective, the maximum heating rate measured by the embedded thermocouple (dT/dt_{max}) reflected the speed at which the sample undergoes thermal decomposition, offering insight into the potential for sudden or accelerated combustion events.
- *Exhaust Gases* were also assessed using a dual perspective. Mass-based indicators included the CO yield (y_{CO}) and the specific extinction area (SEA) directly obtained by the cone calorimeter. SEA quantifies the amount of optically active smoke generated per unit mass of material consumed. High SEA values indicate intense devolatilisation and fragmentation processes, leading to the rapid formation of large quantities of hot exhaust gases. From a physical standpoint, this behaviour is associated with enhanced plume development and convective transport, increasing the thermal and visibility-related load carried by the exhaust flow, thus having a detrimental effect on evacuation. On the other hand, thermal-based indicators were derived from the maximum temperature observed in the exhaust gas plume via infrared thermography (T_{max}), representing the thermal intensity of the emissions and the rate of energy release into the surrounding environment.

For each parameter, values obtained at the different radiant heat fluxes (7, 25, and 50 kW/m^2) were first normalised with respect to the most severe condition observed within the dataset for the same metric. This step ensured that all indicators were expressed on a common, dimensionless scale ranging from 0 to 1, where higher values consistently correspond to a more pronounced manifestation of the underlying physical phenomenon. Importantly, the normalisation was performed across solvents, thereby preserving the comparative nature of the analysis and preventing artificial inflation or suppression of differences arising from flux-dependent scaling effects. In the absence of established threshold values or benchmarks for the process conditions and metrics considered here, the analysis was intentionally formulated as an internal, relative comparison, aimed at highlighting differences in response pathways within the investigated system rather than defining absolute safety limits. Nevertheless, the proposed approach can also be employed

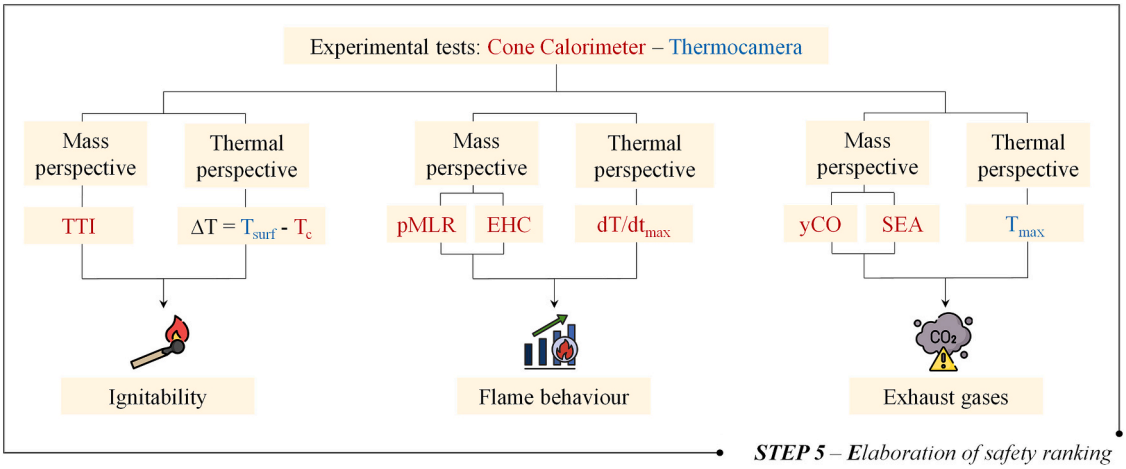

Fig. 3. Schematic representation of the developed safety ranking approach.

for screening scopes if specific threshold values are available and acceptance criteria are posed. The influence of the external heat flux was then incorporated by treating the individual flux conditions as parallel observations of the same material response, rather than as independent safety scenarios. For each solvent and for each safety aspect, the normalised parameter values obtained at different heat fluxes were therefore combined through an arithmetic averaging procedure. This approach reflects the intent of the methodology: to characterise the overall tendency of a given formulation to exhibit critical behaviours under a range of representative thermal loads, rather than to bias the ranking toward a single extreme condition. At a conceptual level, the resulting safety indicator for a given aspect can be expressed in the following generic form:

$$S = \frac{1}{N} \sum_{i=1}^{N} \left(\frac{X_i}{X_{ref}} \right) \quad (1)$$

where X denotes the value of a given safety-relevant parameter measured (S) at the i-th heat flux, X_{ref} is the reference value used for normalisation (corresponding to the most severe case observed for that parameter), and N is the number of imposed heat fluxes. For the sake of clarity, Fig. 3 depicts a schematic representation of the methodology applied in Step 5.

3. Results and discussion

To rationalise the multiscale and multi-parameter nature of membrane fabrication and performance, the considered parameters were organised into a hierarchical structure, schematically illustrated in Fig. 4. The concentric layout is used to emphasise the functional role of the different variables considered and their relative proximity to the final membrane performance objectives. At the core of the scheme lie the target properties of permeance and selectivity, which represent the ultimate functional objectives of the membrane from the perspective of performance. The intermediate layer groups the monitoring parameters, namely the physically measurable structural, chemical, and mechanical characteristics that directly govern gas transport through the carbon network. These attributes reflect the effective membrane quality resulting from the fabrication and conversion process. The outer layer collects the influencing parameters, which operate at the formulation and processing level and indirectly affect performance by steering the evolution of the monitoring parameters. The presented organisation clarifies the relationships between process variables, membrane attributes, and target performance, and provides a visual rationale for the interaction matrices discussed in the following section. The hierarchical structure reported in Fig. 4 is based on a semi-quantitative aggregation of interaction strengths derived from the REC scoring framework, which enables the identification of influencing parameters as net drivers, monitoring parameters as intermediate state variables with the highest interaction density, and target parameters as final measurable outputs.

3.1. Matrix of interactions

Based on the proposed methodology and the considerations reported for the analysed case study, to formalise the relationships among attributes, Table 2 introduces an interaction matrix of the principal influencing parameters. This matrix outlines the relative interaction strength and underlying mechanisms between each pair of parameters, providing a structured framework to interpret how their collective interplay shapes the final membrane quality.

The monitoring parameters included in the interaction matrix were selected because they collectively capture the structural, chemical, and mechanical features that most strongly dictate gas transport in carbon membranes. Their interplay defines both the ease with which molecules traverse the carbon network and the sharpness with which the membrane discriminates among species of different size or affinity. Pore size, porosity fraction, and pore tortuosity constitute the primary descriptors of the internal architecture. Pore size governs molecular restriction, porosity fraction modulates the accessible free volume, and tortuosity shapes the effective diffusion pathways [36]. Their interactions therefore dominate the development of permeance and selectivity, as small alterations in these elements propagate directly into the membrane's transport behaviour [37]. For the sake of clarity, permeance represents the normalised transport capability of the membrane, quantifying the flux of a given species per unit driving force, whereas selectivity expresses the membrane's intrinsic ability to preferentially transport one species over another as a result of differences in diffusivity and sorptive interactions within the microporous carbon network; concise definitions and governing expressions are provided in the current literature [38,39]. Thickness, surface smoothness, and chemical composition introduce additional layers of structural refinement. Thickness determines the diffusion length, surface smoothness influences the uniformity of transport-active regions, and chemical composition affects the balance between adsorption and diffusion within the evolving carbon framework [40,41]. Through these mechanisms, each parameter subtly redefines how transport and discrimination unfold at the microscale. Mechanical integrity provides the overarching constraint that preserves the intended transport mechanism. By preventing crack formation and bypass pathways, it ensures that permeance and selectivity emerge from the designed microporous architecture rather than from defect-driven artefacts [42]. Taken together, the matrix highlights how membrane performance arises from the coordinated evolution of these

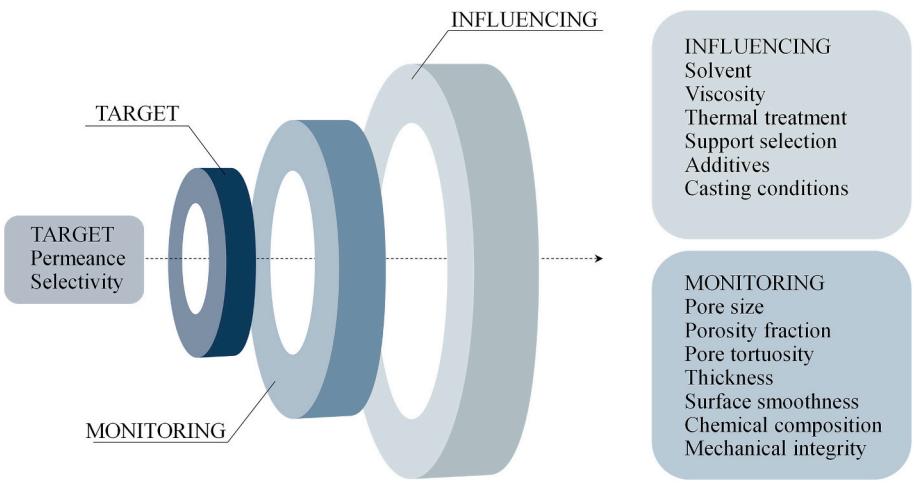

Fig. 4. Hierarchical scheme linking target performance metrics, monitoring parameters, and influencing process variables in carbon membrane production.

Table 2
Interaction matrix of principal monitoring parameters for carbon membrane products. Each cell denotes the interaction strength (Strong/Medium/Weak) between physically measurable characteristics and the underlying mechanism, with explicit reference to their influence on permeance and selectivity. To avoid duplicates, grey boxes were included.

	Pore Size	Porosity Fraction	Pore Tortuosity	Thickness	Surface Smoothness	Chemical Composition	Mechanical Integrity
Pore Size	—	Medium; void-volume (↑permeance)	Strong; path-dimension (↑permeance, ↑selectivity via size exclusion)	Medium; penetration-depth (modulates permeance)	Medium; pore-exposure (minor effect selectivity)	Medium; chemistry-modulated porosity (affects selectivity)	Strong; defect-sensitivity (leakage, reduces selectivity)
Porosity Fraction	—	—	Strong; void-network (↑permeance)	Medium; porosity-gradient (modulates permeance)	Medium; surface-porosity (minor effect selectivity)	Weak; composition-gradient (modulates selectivity slightly)	Strong; structural-porosity (leakage paths, reduces selectivity)
Pore Tortuosity	—	—	—	Strong; flow-path-length (modulates permeance)	Medium; open-pore-exposure (surface interaction)	Medium; transport-exposure (affects selectivity)	Strong; crack-propagation (bypass risk)
Thickness	—	—	—	—	Medium; planar-uniformity (minor effect on flux uniformity)	Weak; composition-gradient (minor effect on selectivity)	Strong; load-bearing (prevents structural failure affecting flux)
Surface Smoothness	—	—	—	—	—	Medium; exposure-area (affects selectivity)	Strong; crack-initiation (creates bypass paths)
Chemical Composition	—	—	—	—	—	—	Medium; network-cohesion (flux stability and selectivity)
Mechanical Integrity	—	—	—	—	—	—	—

attributes, each one shaping and being shaped by the others throughout the transformation from polymer precursor to functional carbon material. This interconnected behaviour also reflects the extent to which the final membrane structure remains sensitive to the underlying conditions that steer its development, a point that becomes increasingly evident when examining the variables that actively drive these transformations. Recognising how these attributes co-evolve highlights the importance of distinguishing the parameters used to assess the final membrane quality from the process variables that steer their development. Table 3 formalises this distinction, contrasting the monitoring parameters with the influencing ones.

The interaction scheme presented in Table 3 illustrates how each influencing variable contributes to the development of the monitoring parameters that ultimately define CMs quality. Rather than acting independently, these variables shape the membrane through a sequence of tightly interconnected mechanisms, from polymer dissolution to film formation and carbonisation, so that modifications introduced at early stages propagate across the entire set of structural and transport-relevant attributes.

Within this framework, the solvent system plays a particularly formative role, as it dictates the initial polymer–solvent interactions, chain mobility, and the thermodynamic pathway leading to pore generation. A solvent such as *N*-methyl-2-pyrrolidone (NMP), representative of class A in the matrix, offers strong solvation and produces highly homogeneous precursor solutions; this determines the scale and regularity of phase separation, with direct consequences for pore size, porosity fraction, surface smoothness, and the eventual diffusion pathways [43]. Greener solvents such as γ-valerolactone (GVL), corresponding to class B, reorganise these mechanisms differently: their solvation strength, volatility, and miscibility with nonsolvent phases shift the kinetics of structure formation and give rise to distinctive pore architectures. The membrane performances of novolac-based carbon membranes prepared using GVL have been previously investigated by the authors and demonstrated to be suitable for the intended application [44]. For the sake of completeness, a summary of the main permeance and selectivity results from that study is exclusively provided in the supplementary material to better focus on the safety and sustainability implications associated with solvent substitution. These differences, already encoded in the matrix, highlight that solvent substitution is never merely compositional but structural, influencing the entire trajectory through which permeance and selectivity emerge. Other influencing parameters intervene at complementary stages. Solution rheology governs the mobility of polymer chains and the rate at which concentration gradients relax, affecting both pore connectivity and tortuosity. Casting conditions modulate the formation of the wet film, controlling thickness, surface texture, and the spatial distribution of nascent carbon domains [45,46]. Support selection determines how stresses, adhesion, and drainage behaviour shape the lower interface of the forming membrane, thereby influencing defect formation and local structural uniformity [47]. During later stages, the thermal-treatment schedule defines the extent of shrinkage, densification, and rearrangement of carbon domains, while additives introduce controlled local perturbations that may stabilise or intentionally modify the evolving network [48,49]. These interactions collectively explain why no single monitoring parameter can be understood in isolation: each reflects the cumulative effects of a multistep process, where several influencing variables may converge on the same structural outcome. When read through this logic, the matrix reveals a natural hierarchy among the influencing parameters, with the solvent system effectively setting the initial thermodynamic and molecular landscape to which all subsequent processing steps must adapt. In practice, many downstream effects, whether rheological, morphological, or interfacial, are conditioned by

Table 3
Interaction matrix that relates monitoring parameters (rows) to influencing parameters (columns), providing a concise overview of the main mechanistic pathways through which controllable process variables shape the resulting material properties.

Monitoring \ Influencing	Solvent A (high-affinity, polar aprotic)	Solvent B (moderate-affinity, less polar, greener)	Viscosity	Thermal Treatment	Support Selection	Additives	Casting Conditions
Pore Size	Strong; high solubility (regular pore formation)	Medium; moderate solubility (heterogeneous pores)	Medium; diffusion-limited pore evolution	Strong; pore expansion/shrinkage	Medium; pore development	Medium; stabilizes walls, slight effect on size	Medium; initial pore orientation (shear/stretch)
Porosity Fraction	Strong; favors open network	Medium; less uniform network	Medium; pore connectivity (high viscosity)	Strong; densification or collapse (higher T)	Medium; modulates void fraction	Medium; enhances or blocks porosity locally	Medium; modulates void fraction
Pore Tortuosity	Medium; linear pore paths	Medium; more convoluted paths	Strong; longer flow paths (viscous solutions)	Medium; stress-induced tortuosity	Weak; path orientation	Weak; minor influence on tortuosity	Medium; pore alignment
Thickness	Medium; solution penetration depth	Medium; less uniform thickness	Strong; film thickness	Medium; shrinkage	Weak; minor effect	Weak; minor effect on uniformity	Strong; baseline thickness (speed)
Surface Smoothness	Strong; smoother surfaces	Medium; rougher surfaces (moderate solubility)	Medium; micro-roughness (high viscosity)	Medium; micro-roughness (thermal contraction)	Weak; minor effect	Medium; roughen surface (additive deposition)	Strong; texture (casting and demolding)
Chemical Composition	Medium; solvent-polymer network	Medium; slight composition variation (different solvation)	Weak; viscosity indirect	Medium; side reactions	Medium; substrate interactions	Strong; direct chemical modification	Medium; interactions with mold/support
Mechanical Integrity	Medium; network strength	Medium; local weaknesses (heterogeneous morphology)	Strong; fewer defects (high viscosity)	Strong; stress relaxation, prevents cracking (T control)	Medium; substrate rigidity	Medium; reinforce or weaken	Medium; casting defects (stress concentrators)

this initial environment, such that variations introduced later in the process tend to refine, rather than redefine, the structural trajectory established at the dissolution and phase-inversion stages. Seen in this broader context, the solvent system remains a central element since it determines the very starting point from which all subsequent structure-forming events unfold. Its thermochemical behaviour also has safety implications. While widely used solvents such as NMP have well-established thermal-decomposition profiles, greener candidates such as GVL, although promising from a sustainability perspective, lack a comparable body of safety data. Differences in volatility, decomposition onset, and by-product formation may alter not only membrane morphology but also the conditions experienced during thermal treatment. The following section focuses precisely on this aspect, using controlled thermal-stress testing to clarify how alternative solvents behave during processing and to assess whether their structural advantages can be pursued without compromising operational safety.

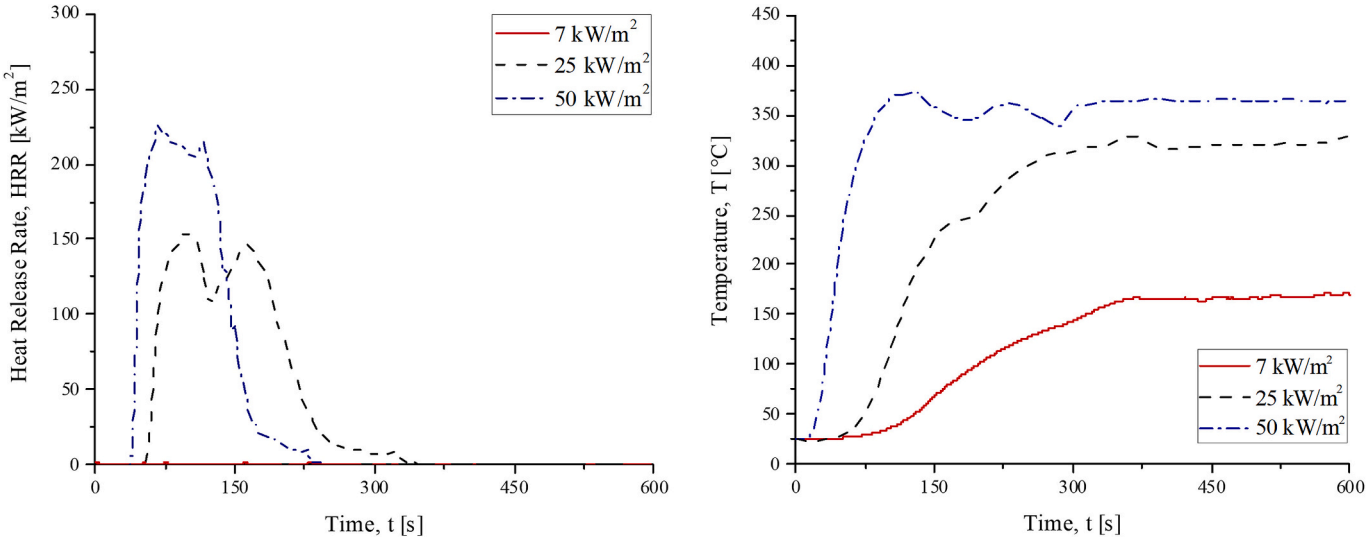

Fig. 5. Heat release rate profile (left) and temperature profile (right) over time of novolac samples at 7, 25 and 50 kW/m^2.

3.2. Safety-based ranking

Cone calorimetry was employed as the main diagnostic tool, as it provides quantitative insight into the combustion dynamics of polymeric materials, including ignition time, heat release rate (HRR), and thermal stability. The investigation was first conducted on pristine novolac resin, which served as the baseline reference, and subsequently extended to novolac-based solutions with GVL and NMP. The following section discusses the response of these materials under controlled cone calorimeter conditions, highlighting both the intrinsic fire performance of novolac and the effect of solvent-derived modifications. Fig. 5 reports the corresponding heat release rate (left) and the temperature profile recorded close to the bottom of the specimen (right), which together provide a comprehensive view of the combustion dynamics and internal heat transfer.

Once 25 kW/m^2 is provided to the sample, the HRR evolution of novolac displays a clear two-step pattern. Shortly after ignition, a sharp maximum of approximately 150 kW/m^2 is observed, reflecting the intense release and combustion of degradation volatiles generated in the early stages of decomposition. After a short decline, a second broader maximum of about 140 kW/m^2 emerges, sustained by the progressive involvement of the bulk material. The absence of a stable plateau between the two maxima suggests that these processes are partially overlapping, with heat feedback from the flame accelerating the decomposition front inside the sample. Such a two-step combustion profile is characteristic of phenolic novolac, where an initial devolatilization phase is followed by the breakdown of more condensed aromatic domains, as consistently reported in the literature [50]. Conversely, the single HRR peak observed at 50 kW/m^2 indicates that the increased thermal input accelerates the propagation of the decomposition front through the sample, resulting in a substantial overlap of the degradation stages that remain distinguishable at 25 kW/m^2. The temperature profiles measured near the sample base exhibit distinct behaviour depending on the applied heat flux. At 7 kW/m^2, the temperature rapidly reaches a plateau around 120 °C, which persists for approximately 1000 s. Under these conditions, the novolac sample does not ignite, even with the use of the external spark igniter, as confirmed by the negligible HRR values. This indicates that, although initial heating and devolatilization occur, self-sustained combustion does not take place, consistent with the negligible HRR observed. The plateau likely corresponds to slow evaporation of early-stage volatile degradation products, without substantial chemical bond scission within the phenolic network. At 25 kW/m^2, the temperature rises more rapidly, reaching a plateau of approximately 300 °C, coinciding with the development of the second HRR peak. At this heat flux, novolac undergoes autoignition, i.e., flaming combustion is established without activation of the spark igniter, indicating that the material attains a thermal condition sufficient to trigger the decomposition of the more stable aromatic domains within the novolac resin. Physically, this plateau reflects local softening typical of amorphous thermosetting polymers under heating, which facilitates the inward propagation of the decomposition front. Chemically, the elevated temperature promotes cleavage of bonds within the phenolic network and enhances the release of combustible gaseous products. The combined analysis of HRR and temperature profiles reveals a two-stage degradation process. The first stage involves the rapid release of volatiles, which is partially activated even at low fluxes but does not sustain combustion. The second stage, observable at higher fluxes, corresponds to advanced decomposition of the bulk material, characterised by the breakdown of condensed aromatic structures and the associated increase in HRR. Notably, the time required to reach each plateau is similar across fluxes, indicating that the kinetics of initial heating are comparable, while the extent of thermal activation governs the onset of significant combustion. Overall, the interplay between HRR evolution and temperature plateaus allows us to reconstruct the thermochemical behaviour of novolac resin: an early devolatilization phase at lower temperatures and heat fluxes, followed by an advanced decomposition phase at elevated temperatures. The fire response of the dipping solutions, identified as the most critical step of the membrane preparation process due to the presence of flammable solvents and the subsequent thermal treatment, reveals distinct behaviours depending on the solvent employed. Fig. 6 presents the heat release rate (HRR) profiles of novolac–NMP mixtures under different external heat fluxes. Table 4 reports the main thermal parameters obtained from the experimental tests: peak heat release rate (pHRR), mean heat release rate (HRR mean), peak mass loss rate (pMLR), mass loss rate at the steady state (MLR), peak CO production rate (pCOP), peak CO_2 production rate (pCO2P), mean CO production rate (COP), mean CO_2 production rate (CO_2P), mean effective heat of combustion (EHC mean), and time to ignition (TTI). Parameters denoted with p refer to the maximum values reached during combustion, while the mean values are reported under quasi-steady conditions, whenever such a regime could be identified.

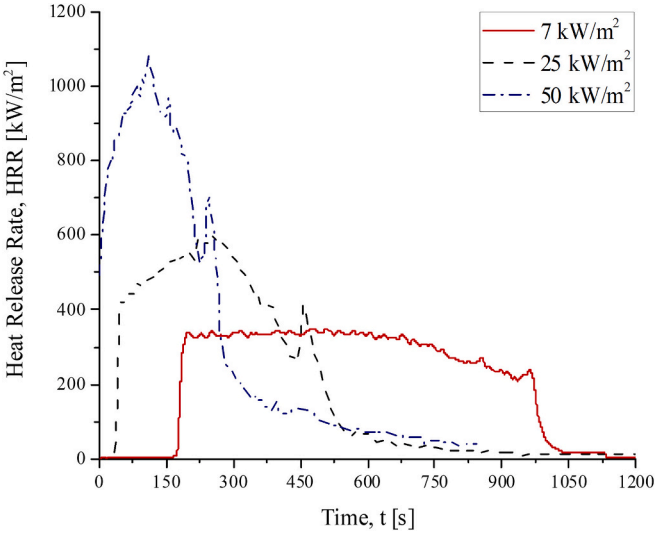

Fig. 6. Heat release rate profiles of novolac-NMP samples at different heat fluxes (7,25, and 50 kW/m^2).

For the novolac/NMP solution, the HRR evolution under external irradiation displays a pronounced single-step profile, with a sharp increase leading to peak values of approximately 1020 kW/m^2 at 50 kW/m^2 flux. At intermediate fluxes (25 kW/m^2), the maximum HRR is reduced by nearly half, while at the lowest flux (7 kW/m^2) only a modest release of energy is observed. At 7 kW/m^2, flaming combustion is established only after activation of the external spark igniter, whereas at 25 and 50 kW/m^2 the system undergoes autoignition under external irradiation. The short time to ignition can be attributed to the high volatility and low thermal stability of NMP, which promotes rapid vapor release upon heating and triggers combustion almost immediately after exposure to external irradiation. As a result, the degradation of the phenolic resin is no longer expressed through the two-step sequence typical of pure novolac, but is instead masked by a solvent-driven volatilisation front. The combustion becomes strongly exothermic in the initial stage, with little evidence of a progressive involvement of the bulk material. Mechanistically, this indicates that NMP destabilises the thermal resistance of the system, coupling rapid solvent evaporation with early bond cleavage in the novolac network, which explains the abrupt and uncontrolled HRR spikes observed. Furthermore, the HRR exhibits a relatively prolonged plateau (extended steady-state combustion stage), indicating sustained energy release over time. During the gas-phase combustion, potentially toxic species such as NOx may be formed, highlighting an important consideration for process safety.

In comparison, the novolac/GVL solution (Fig. 7 and Table 5) exhibits a markedly different combustion pattern. For all the investigated heat fluxes (7–25–50 kW/m^2), flaming combustion is achieved only

Table 4
Main thermal parameters obtained from cone calorimeter tests of novolac/NMP formulation at different heat fluxes (7, 25, and 50 kW/m^2). The reported values refer to quasi-steady conditions, while parameters denoted with p refer to the maximum values.

	Ignited 7 kW/m^2	Autoignited 25 kW/m^2	Autoignited 50 kW/m^2
pHRR [kW/m^2]	352.2	612.1	1088
HRR [kW/m^2]	336.5	582.1	1020
pMLR [g/s]	0.128	0.2	0.362
MLR [g/s]	0.118	–	–
pCOP [g/s]	0.003	0.008	0.02
pCO2P [g/s]	0.237	0.431	0.788
COP [g/s]	0.001	0.001	0.002
CO2P [g/s]	0.227	0.413	0.753
EHC [MJ/g]	28.9	29.3	28.5
TTI [s]	180	40	1

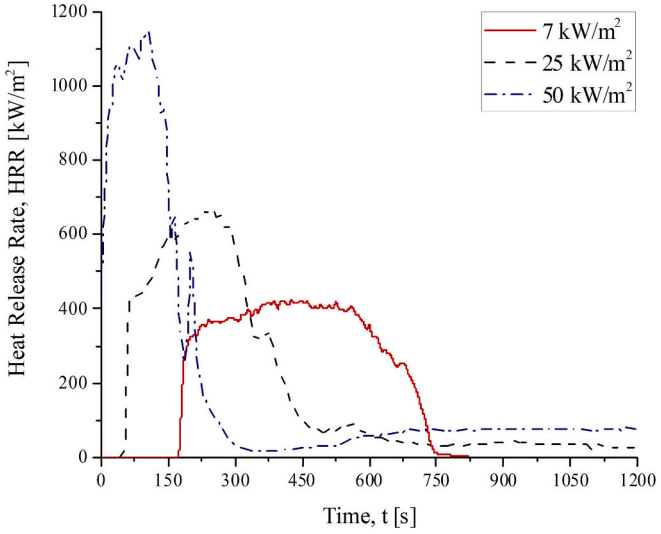

Fig. 7. Heat release rate profiles of novolac-GVL samples at different heat fluxes (7–25-50 kW/m^2).

Table 5
Main thermal parameters obtained from cone calorimeter tests of novolac/GVL formulation at different heat fluxes (7–25-50 kW/m^2). The reported values refer to quasi-steady conditions, while parameters denoted with p refer to the maximum values.

	Ignited 7 kW/m^2	Autoignited 25 kW/m^2	Autoignited 50 kW/m^2
pHRR [kW/m^2]	431.0	674.0	1149
HRR [kW/m^2]	411.0	648.0	1111
pMLR [g/s]	0.232	0.320	0.473
MLR [g/s]	0.165	–	0.479
pCOP [g/s]	0.003	0.005	0.016
pCO2P [g/s]	0.339	0.545	0.999
COP [g/s]	0.003	0.004	0.016
CO2P [g/s]	0.327	0.526	0.955
EHC [MJ/g]	20.90	21.9	20.18
TTI [s]	180	60	1

upon activation of the external spark igniter, indicating the absence of autoignition under the tested conditions. At 50 kW/m^2, the HRR curve shows a sharp initial maximum of about 1149 kW/m^2, followed by a rapid decline, indicating a solvent-dominated combustion stage. At lower fluxes (25 and 7 kW/m^2), the HRR maxima decrease substantially (111 and 431 kW/m^2, respectively), and the overall burning duration is considerably shorter than in the NMP-based solution. The slightly higher HRR peaks compared to NMP can be attributed to the oxygenated nature of GVL, which facilitates more complete oxidation of the solvent vapors and enhances CO and CO_2 production. This also leads to a faster heat feedback to the resin surface, accelerating the initial decomposition of the aromatic domains in novolac. Overall, the novolac/GVL solution exhibits a combustion profile characterised by shorter duration and sharper peaks. The absence of a prolonged plateau, unlike in NMP, reflects a more transient energy release: the rapid volatilisation of GVL quickly triggers the initial decomposition of the polymer, but the lower volatility compared to NMP prevents a sustained combustion phase. Consequently, the resin burns rapidly at first, but the reaction does not continue for an extended period. Mechanistically, this suggests that while the decomposition of condensed aromatic domains is initiated efficiently, the energy release is concentrated in the early stage. Importantly, the absence of highly toxic gas-phase species during GVL combustion further indicates that the solvent promotes efficient thermal decomposition of the novolac matrix. The absence of highly toxic gas-phase species makes GVL a safer solvent in terms of process hazards.

Taken together, the comparative analysis shows that solvent choice fundamentally alters the thermal–chemical degradation pathway of the dipping solutions. While HRR values for GVL are slightly higher, reflecting its oxygenated nature, NMP maintains an extended steady-state HRR stage, but with the additional risk of generating toxic compounds. Therefore, from a process safety perspective, GVL presents a lower chemical hazard despite comparable energy release, whereas NMP requires careful handling to mitigate the formation of harmful gaseous species during combustion.

The collected data allow us to move beyond a purely descriptive comparison of combustion profiles and extract safety-relevant insights applicable to processing conditions. Table 6 reports the obtained indicators in order to assess the ignitability, the flame behaviour and exhaust gases of the two formulations under examination, from both mass- and thermal-based perspectives. The corresponding data resolved by individual external heat flux (7, 25 and 50 kW/m^2) are reported in dedicated tables in the Supplementary Material.

For the novolac–NMP formulation, ignition-related indicators remain systematically elevated over the entire heat-flux range, reflecting a strong propensity toward rapid activation once a critical thermal threshold is reached. This behaviour is attributable to the short ignition times and weak thermal inertia observed experimentally, and it indicates that the dominant hazard pathway for NMP-based solutions is associated with early-stage solvent-driven volatilisation, largely insensitive to the external heat flux once ignition is achieved. In contrast, the novolac–GVL system exhibits a more flux-dependent ignition response, with intermediate heat fluxes producing comparatively lower ignition-related scores. This trend suggests a greater thermal buffering capacity and a delayed transition toward sustained combustion, in line with the higher boiling point and lower volatility of GVL. As a result, ignition in GVL-based solutions appears to be governed by a thermally mediated activation pathway, rather than by immediate solvent evaporation. Differences between the two systems become more pronounced when flame-intensity indicators are examined. While both formulations reach high peak values at elevated heat fluxes, the NMP-based solution consistently shows higher scores associated with sustained mass-loss and extended heat-release plateaus, indicating prolonged energy delivery to

Table 6
Comparison of NMP and GVL formulations in terms of ignitability, flame behaviour, and exhaust gases characteristics.

	Solvent A = Novolac/NMP		Solvent B = Novolac/GVL	
	Mass Perspective	Thermal Perspective	Mass Perspective	Thermal Perspective
Ignitability	1.00	1.00	0.89	0.86
Flame behaviour	0.82	0.98	0.86	0.91
Exhaust Gas	0.98	1.00	0.69	0.86
Overall	0.96		0.85	

the system. This sustained regime implies a hazard pathway dominated by continuous fuel supply, which may amplify thermal feedback during processing. Conversely, the GVL-based formulation is characterised by sharper but shorter-lived intensity indicators, with a significantly reduced duration of the active combustion stage (e.g., time interval between ignition and extinction), which decreases from values exceeding ~900 s for NMP-based systems to ~600 s for GVL-based systems under comparable heat flux conditions (7 kW/m^2). Such behaviour points to a pulse-like combustion pathway, where rapid solvent involvement does not translate into long-lasting thermal stress on the material. The evolution of gaseous products further reinforces this trend. For NMP, hot gases are generated continuously and in large quantities, extending the energetic impact on the surrounding environment. GVL moderates both the timing and intensity of gas release, leading to a more controlled development of hot plumes. Overall, the aggregated indicators highlight that the GVL-based formulation exhibits a lower global severity compared to NMP. This improvement arises from a combination of factors: delayed ignition due to higher boiling point and lower volatility, sharper but shorter flame peaks that limit sustained heat release, and a moderated generation of hot gaseous products. Collectively, these effects reduce the thermal feedback to the material and limit the propagation of solvent-driven volatilisation, providing a more controlled thermal response under external irradiation.

4. Conclusion

This work presents a rigorous and systematic methodology for the early-stage assessment of inherent safety and performance in the development of innovative chemical processes, integrating mechanistic reasoning, experimental validation, and structured interaction mapping. The proposed SCALE workflow enables the identification of critical monitoring parameters and their influencing variables, providing a clear framework to understand how process conditions shape final material properties. Applied to the production of carbon membranes, the approach revealed the hierarchical interplay between structural, chemical, and mechanical characteristics, and demonstrated how solvent choice and processing conditions collectively guide pore formation, surface morphology, and overall membrane quality. Thermal-stress testing of novolac-based dipping solutions highlighted the significant impact of solvent properties on ignition behaviour, flame intensity, and exhaust-gas generation. In particular, replacing NMP with GVL led to moderated ignition propensity, with ignitability indicators reduced from 1.00 to 0.89 (mass-based) and from 1.00 to 0.86 (thermal-based), shorter and less sustained flame events, and a reduction in smoke and exhaust-gas severity, with exhaust-gas indicators decreasing from 0.98 to 0.69 (mass-based) and from 1.00 to 0.86 (thermal-based). Despite comparable peak heat release rates at high heat flux (pHRR ≈ 1088 kW/m^2 for NMP and ≈ 1149 kW/m^2 for GVL at 50 kW/m^2), GVL exhibited a more transient combustion behaviour, limiting prolonged thermal exposure. Overall, the integrated safety ranking confirms that the GVL-based formulation achieves a lower global hazard level, with an overall safety indicator reduced from 0.96 (NMP) to 0.85 (GVL), while maintaining process effectiveness. The integration of systematic interaction mapping with targeted experimental evaluation therefore provides a powerful tool to guide the development of safer and more sustainable processes, offering insights that are broadly applicable to other polymer-based systems and thermal-treatment operations.

CRediT authorship contribution statement

Benedetta A. De Liso: Writing – original draft, Investigation, Formal analysis, Data curation. **Clara Coiana:** Writing – review & editing, Visualization. **Gianmaria Pio:** Writing – review & editing, Supervision, Methodology, Conceptualization. **Fausto Gallucci:** Writing – review & editing, Validation, Supervision. **Ernesto Salzano:** Writing – review & editing, Supervision, Resources, Project administration.

Declaration of competing interest

The authors declare that they have no known competing financial interests or personal relationships that could have appeared to influence the work reported in this paper.

Appendix A. Supplementary data

Supplementary data to this article can be found online at https://doi.org/10.1016/j.cej.2026.179153.

Data availability

Data will be made available on request.

References

[1] The pathway to process scale-up, Nat. Chem. Eng. 1 (2024) 387–388, https://doi.org/10.1038/s44286-024-00086-6.
[2] D.A. Crowl, J.F. Louvar, Chemical Process Safety, 2002.
[3] I. Rossetti, M. Compagnoni, Chemical reaction engineering, process design and scale-up issues at the frontier of synthesis: flow chemistry, Chem. Eng. J. 296 (2016) 56–70, https://doi.org/10.1016/j.cej.2016.02.119.
[4] F. Zanobetti, G. Pio, S. Jafarzadeh, M.M. Ortiz, V. Cozzani, Inherent safety of clean fuels for maritime transport, Process Saf. Environ. Prot. 174 (2023) 1044–1055, https://doi.org/10.1016/j.psep.2023.05.018.
[5] P.A. Carson, C.J. Mumford, Hazardous Chemicals Handbook, 2013, https://doi.org/10.1016/C2009-0-24010-4.
[6] F. Sun, W. Xu, G. Wang, N. Shi, Z. Yang, Development of a hazard index for reactivity management (HIRM) in chemical process, Process Saf. Environ. Prot. 149 (2021) 22–34, https://doi.org/10.1016/j.psep.2020.10.018.
[7] A. Kummer, T. Varga, What do we know already about reactor runaway? – a review, Process. Saf. Environ. Prot. 147 (2021) 460–476, https://doi.org/10.1016/j.psep.2020.09.059.
[8] J. Jiang, J. Jiang, Y. Pan, R. Wang, P. Tang, Investigation on thermal runaway in batch reactors by parametric sensitivity analysis, Chem. Eng. Technol. 34 (2011) 1521–1528, https://doi.org/10.1002/ceat.201000517.
[9] K.R. Westerterp, E.J. Molga, No more runaways in fine chemical reactors, Ind. Eng. Chem. Res. 43 (2004) 4585–4594, https://doi.org/10.1021/ie030725m.
[10] D.W. Mosley, A.I. Ness, D.C. Hendershot, Screen reactive chemical hazards early in process development, Chem. Eng. Prog. 96 (2000) 51–63.
[11] Q. Yang, J. Wang, X. Chen, S. Yang, S. Huo, Q. Chen, P. Guo, X. Wang, F. Liu, W. Chen, P. Song, H. Wang, A phosphorus-containing tertiary amine hardener enabled flame retardant, heat resistant and mechanically strong yet tough epoxy resins, Chem. Eng. J. 468 (2023), https://doi.org/10.1016/j.cej.2023.143811.
[12] L.Y. Jiang, Z. Li, Y.M. Liang, Q.Q. Bi, S. Tian, S.Y. Lin, Z. Hu, Y. Zheng, J. Hobson, D.Y. Wang, High-efficient fire-safe epoxy enabled by bio-based atomic-level catalytic engineering, Chem. Eng. J. 461 (2023), https://doi.org/10.1016/j.cej.2023.141967.
[13] G. Schinazi, E.J. Price, D.A. Schiraldi, Fire testing methods of bio-based flame-retardant polymeric materials, in: bio-based flame-retardant Technol. Polym. Mater., 2022, pp. 61–95, https://doi.org/10.1016/B978-0-323-90771-2.00009-2.
[14] J.G. Q., B.P. D., R.E. L., An Investigation of the UL-94V Plastics Flammability Test, 2011, pp. 1020–1031, https://doi.org/10.3850/978-981-08-7724-8_15–03.
[15] T.R. Hull, Challenges in fire testing: reaction to fire tests and assessment of fire toxicity, in: Adv. Fire Retard. Mater., 2008, pp. 255–290, https://doi.org/10.1533/9781845694701.2.255.
[16] F. Gallucci, S. Poto, M.A.L. Tanco, D.A. Pacheco Tanaka, Production of methanol by CO2 hydrogenation using a membrane reactor, Catalysts 16 (2026) 53, https://doi.org/10.3390/catal16010053.
[17] M. Deng, J. Wei, Y. Ma, Z. Qin, J. Song, L. Yang, L. Yao, W. Jiang, S. Yi, N. Li, Z. Dai, Next-generation carbon molecule sieve membranes derived from polyimides and polymers of intrinsic microporosity for key energy intensive gas separations and carbon capture, J. Mater. Chem. A 12 (2024) 19806–19838, https://doi.org/10.1039/d4ta02112f.
[18] T. Harlacher, M. Wessling, Gas-gas separation by membranes, in: Prog. Filtr. Sep., 2015, pp. 557–584, https://doi.org/10.1016/B978-0-12-384746-1.00013-6.
[19] H.T. Lu, W. Li, E.S. Miandoab, S. Kanehashi, G. Hu, The opportunity of membrane technology for hydrogen purification in the power to hydrogen (P2H) roadmap: a review, Front. Chem. Sci. Eng. 15 (2021) 464–482, https://doi.org/10.1007/s11705-020-1983-0.
[20] S. Poto, A. Aguirre, F. Huigh, M.A. Llosa-Tanco, D.A. Pacheco-Tanaka, F. Gallucci, M.F. Neira d'Angelo, Carbon molecular sieve membranes for water separation in CO2 hydrogenation reactions: effect of the carbonization temperature, J. Membr. Sci. 677 (2023), https://doi.org/10.1016/j.memsci.2023.121613.
[21] A. Rahimalimamaghani, D.A. Pacheco Tanaka, M.A. Llosa Tanco, F. Neira D'Angelo, F. Gallucci, New hydrophilic carbon molecular sieve membranes for bioethanol dehydration via pervaporation, Chem. Eng. J. 435 (2022), https://doi.org/10.1016/j.cej.2022.134891.

[22] A.F. Ismail, L.I.B. David, A review on the latest development of carbon membranes for gas separation, J. Membr. Sci. 193 (2001) 1–18, https://doi.org/10.1016/S0376-7388(01)00510-5.
[23] L. Lei, L. Bai, A. Lindbråthen, F. Pan, X. Zhang, X. He, Carbon membranes for CO2 removal: status and perspectives from materials to processes, Chem. Eng. J. 401 (2020), https://doi.org/10.1016/j.cej.2020.126084.
[24] L. Forster, C. D'Agostino, M.A. Llosa-Tanco, V. Spallina, C. Brencio, F. Gallucci, M. Lindley, S.J. Haigh, D.A. Pacheco-Tanaka, Tailoring pore structure and surface chemistry of microporous alumina-carbon molecular sieve membranes (Al-CMSMs) by altering carbonization temperature for optimal gas separation performance: an investigation using low-field NMR relaxation measurements, Chem. Eng. J. 424 (2021), https://doi.org/10.1016/j.cej.2021.129313.
[25] W.N.W. Salleh, A.F. Ismail, Effects of carbonization heating rate on CO 2 separation of derived carbon membranes, Sep. Purif. Technol. 88 (2012) 174–183, https://doi.org/10.1016/j.seppur.2011.12.019.
[26] T.A. Centeno, J.L. Vilas, A.B. Fuertes, Effects of phenolic resin pyrolysis conditions on carbon membrane performance for gas separation, J. Membr. Sci. 228 (2004) 45–54, https://doi.org/10.1016/j.memsci.2003.09.010.
[27] J.J. Li, W. Wei, Q. Lin, J.Y. Zhang, Effects of pyrolysis temperature on the properties of phenol-formaldehyde resin based carbon molecular sieve membrane, Mater. Sci. Forum 848 (2016) 738–742, https://doi.org/10.4028/www.scientific.net/MSF.848.738.
[28] N. Fatima, H. Waheed, A. Raza, A. Mukhtar, F. Ahmad, A critical review on membrane technology and its application in CO2 capturing, Chem. Methodol. 8 (2024) 662–698, https://doi.org/10.48309/chemm.2024.473209.1818.
[29] S.M. Mousavi, S. Raveshiyan, Y. Amini, A. Zadhoush, A critical review with emphasis on the rheological behavior and properties of polymer solutions and their role in membrane formation, morphology, and performance, Adv. Colloid Interf. Sci. 319 (2023), https://doi.org/10.1016/j.cis.2023.102986.
[30] J. Su, A.C. Lua, Influence of carbonisation parameters on the transport properties of carbon membranes by statistical analysis, J. Membr. Sci. 278 (2006) 335–343, https://doi.org/10.1016/j.memsci.2005.11.017.
[31] ISO 5660, Reaction to fire tests - Heat release, smoke production and mass loss rate, 2019, 2019.
[32] B.A. De Liso, G. Pio, E. Salzano, Small scale pool fires: the case of toluene, J. Loss Prev. Process Ind. 92 (2024), https://doi.org/10.1016/j.jlp.2024.105430.
[33] B.A. De Liso, G. Pio, E. Salzano, Experimental and advanced numerical characterization of toluene fires, Fuel 397 (2025), https://doi.org/10.1016/j.fuel.2025.135448.
[34] B.A. De Liso, G. Pio, E. Salzano, Multicriteria approach to assess the fire behaviour of polymers in electrochemical energy storage, J. Loss Prev. Process Ind. 94 (2025) 105541, https://doi.org/10.1016/j.jlp.2024.105541.
[35] B.A. De Liso, G. Pio, C. Chanut, E. Salzano, Determining the kinetic of the oxidation of metallic solid particles, Chem. Eng. J. 514 (2025), https://doi.org/10.1016/j.cej.2025.163164.
[36] K.M. Steel, W.J. Koros, Investigation of porosity of carbon materials and related effects on gas separation properties, Carbon 41 (2003) 253–266, https://doi.org/10.1016/S0008-6223(02)00309-3.
[37] S. Lagorsse, F.D. Magalhães, A. Mendes, Carbon molecular sieve membranes: sorption, kinetic and structural characterization, J. Membr. Sci. 241 (2004) 275–287, https://doi.org/10.1016/j.memsci.2004.04.038.
[38] A.R. Kamble, C.M. Patel, Z.V.P. Murthy, A review on the recent advances in mixed matrix membranes for gas separation processes, Renew. Sust. Energ. Rev. 145 (2021), https://doi.org/10.1016/j.rser.2021.111062.
[39] Z.E. Sahin, A. Rahimalimamaghani, M. Gazzani, F. Gallucci, Gas permeation through carbon membranes: model development and experimental validation, Int. J. Hydrog. Energy 50 (2024) 561–581, https://doi.org/10.1016/j.ijhydene.2023.08.272.
[40] H. Hatori, Y. Yamada, M. Shiraishi, In-plane orientation and graphitizability of polyimide films: II. Film thickness dependence, Carbon 31 (1993) 1307–1312, https://doi.org/10.1016/0008-6223(93)90090-W.
[41] X. Ma, Y.S. Lin, X. Wei, J. Kniep, Ultrathin carbon molecular sieve membrane for propylene/propane separation, AICHE J. 62 (2016) 491–499, https://doi.org/10.1002/aic.15005.
[42] W. Wei, G. Qin, H. Hu, L. You, G. Chen, Preparation of supported carbon molecular sieve membrane from novolac phenol-formaldehyde resin, J. Membr. Sci. 303 (2007) 80–85, https://doi.org/10.1016/j.memsci.2007.06.055.
[43] M. Teixeira, S.C. Rodrigues, M. Campo, D.A. Pacheco Tanaka, M.A. Llosa Tanco, L. M. Madeira, J.M. Sousa, A. Mendes, Boehmite-phenolic resin carbon molecular sieve membranes-permeation and adsorption studies, Chem. Eng. Res. Des. 92 (2014) 2668–2680, https://doi.org/10.1016/j.cherd.2013.12.028.
[44] C. Coiana, B.A. De Liso, G. De Felice, E. Salzano, F. Gallucci, Green solvents for Novolac-based carbon membranes production, Int. J. Hydrog. Energy 200 (2026), https://doi.org/10.1016/j.ijhydene.2025.152940.
[45] N. Widjojo, T.S. Chung, Pervaporation dehydration of C2-C4 alcohols by 6FDA-ODA-NDA/Ultem® dual-layer hollow fiber membranes with enhanced separation performance and swelling resistance, Chem. Eng. J. 155 (2009) 736–743, https://doi.org/10.1016/j.cej.2009.09.015.
[46] B. Zhang, L. Li, C. Wang, J. Pang, S. Zhang, X. Jian, T. Wang, Effect of membrane-casting parameters on the microstructure and gas permeation of carbon membranes, RSC Adv. 5 (2015) 60345–60353, https://doi.org/10.1039/c5ra10473d.
[47] J.B.S. Hamm, A. Ambrosi, J.G. Griebeler, N.R. Marcilio, I.C. Tessaro, L.D. Pollo, Recent advances in the development of supported carbon membranes for gas separation, Int. J. Hydrog. Energy 42 (2017) 24830–24845, https://doi.org/10.1016/j.ijhydene.2017.08.071.
[48] D.S. Lafyatis, J. Tung, H.C. Foley, Poly(furfuryl alcohol)-derived carbon molecular sieves: dependence of adsorptive properties on carbonization temperature, time, and poly(ethylene glycol) additives, Ind. Eng. Chem. Res. 30 (1991) 865–873, https://doi.org/10.1021/ie00053a008.
[49] M.A. Llosa Tanco, D.A. Pacheco Tanaka, A. Mendes, Composite-alumina-carbon molecular sieve membranes prepared from novolac resin and boehmite. Part II: effect of the carbonization temperature on the gas permeation properties, Int. J. Hydrog. Energy 40 (2015) 3485–3496, https://doi.org/10.1016/j.ijhydene.2014.11.025.
[50] T. Ahamad, S.M. Alshehri, Thermal degradation and evolved gas analysis of epoxy (DGEBA)/novolac resin blends (ENB) during pyrolysis and combustion, J. Therm. Anal. Calorim. 111 (2013) 445–451, https://doi.org/10.1007/s10973-012-2431-2.